# Laser spectroscopy of phonons and rotons in superfluid helium doped with Dy atoms

P. Moroshkin,[1,*] A. Borel,[1,2] and K. Kono[1,3,4]
[1]*RIKEN, CEMS, 2-1 Hirosawa, Wako, 351-0198 Saitama, Japan*
[2]*LPEM, PSL Research University, ESPCI Paris, 10 rue Vauquelin, 75231 Paris Cedex 5, France*
[3]*Institute of Physics, National Chiao Tung University, Hsinchu 300, Taiwan*
[4]*Institute of Physics, Kazan Federal University, Kremlyovskaya st. 18, 420008 Kazan, Russia*

(Received 25 August 2017; published 9 March 2018)

We report the results of a high-resolution laser-spectroscopy study of dysprosium atoms injected into superfluid $^4$He. A special attention is paid to the transitions between the inner $4f$ and $5d$ electronic shells of Dy. The characteristic gap is observed between the zero-phonon line and the phonon wing in the experimental excitation spectrum that arises due to the peculiar structure of the phonon-roton spectrum of superfluid He. This observation resolves the longstanding discrepancy between the studies of bulk superfluid He and He nanodroplets.

DOI: 10.1103/PhysRevB.97.094504

## I. INTRODUCTION

When a metal atom is injected into superfluid helium, it resides in the center of a nanometer-sized cavity formed in the surrounding quantum fluid due to the strong repulsion between He atoms and the foreign atom. The cavity has the shape and the size of the outer electron shell of the embedded atom and is usually referred to as an atomic bubble. Elementary excitations of superfluid He, such as phonons and rotons, couple to various electronic properties of the impurity atom via the vibrations of the bubble surface. This process is of fundamental interest since it represents the interaction between two quantum subsystems: one is microscopic and strongly localized (atom in the bubble); another, delocalized and spread over a macroscopically large volume (quantum fluid He). Understanding of the details of the phonon-impurity coupling mechanism is also essential for the usage of atomic bubbles as microscopic probes for the properties and elementary excitations of quantum fluids and solids and for further studies of microscopic effects of superfluidity.

The structure, energetics, and dynamics of atomic bubbles had been addressed in a number of studies (for a review see Ref. [1]). Optical transitions within the inner electronic shells of the embedded atoms [2–5] are screened from the surrounding He by the valence electrons. In that case the kick on the bubble interface produced by the sudden change of the impurity electron configuration is rather small and the spectrum typically consists of two parts: a zero-phonon line (ZPL) and a phonon wing (PW). The former is a very sharp peak associated with the transitions that involve no creation or annihilation of phonons, i.e., no energy transfer between the dopant and the environment. The latter (PW) appears due to the transitions that generate or annihilate a small number of phonons. The PW line shape thus reflects the spectrum of the generated phonon wave packet [4]. The spectral width of the ZPL is determined by the scattering [6] of the thermal phonons (rotons) on the atomic bubble and by the lifetime of the electronically excited state of the dopant.

A number of experiments reported ZPL and PW in the electronic spectra of various molecules attached to superfluid He nanodroplets (for a review see Refs. [7,8]). Among them, the spectrum of glyoxal had been interpreted in terms of elementary excitations and provided the evidence for the superfluidity of the droplets [9]. The key feature is a 170 GHz (5.6 cm$^{-1}$) gap between the ZPL and PW that arises due to a peculiar structure of the spectrum of elementary excitations in a superfluid that is not expected in normal liquids. Due to the evaporative cooling, the temperature of helium nanodroplets can not be varied that makes it impossible to observe a transition from normal fluid to superfluid phase. Further complications arise due to the anisotropic molecule-helium interaction that is not yet very well characterized, from molecular vibrations and rotations, which also couple to the elementary excitations, and from possible surface-related and finite-size effects due to the small size of the droplets [7,8]. It is therefore important to study the impurity-phonon coupling in bulk superfluid helium, with well-characterized spherical atomic bubbles as impurities.

Several experiments of this kind have been reported up to date. Excitation spectra have been studied for the $4f$-$5d$ inner-shell transitions of lanthanide elements Tm [2] and Eu [3]. In emission, ZPL and PW have been observed for the forbidden $3d$-$4s$ transitions of Cu [10,11] and $5d$-$6s$ transitions of Au [5,11]. No gap had been found between ZPL and PW in those experiments, neither in superfluid nor in normal fluid helium. Although, a well-resolved gap had been observed in solid He samples [5,10,11]. The origin of this discrepancy until now remained unclear.

Here we present a new high-resolution spectroscopic study of dysprosium atoms in bulk superfluid helium that resolves this issue and reports the dependence of the ZPL and PW on temperature and laser power. Dy is a perspective candidate for the low-temperature studies because of its very large magnetic moment. Recently, it was proposed [12] to use Dy atoms embedded into a solid $^4$He matrix to realize a controllable quantum spin glass phase. Presently, there is also a renewed

*petr.moroshkin@riken.jp

 

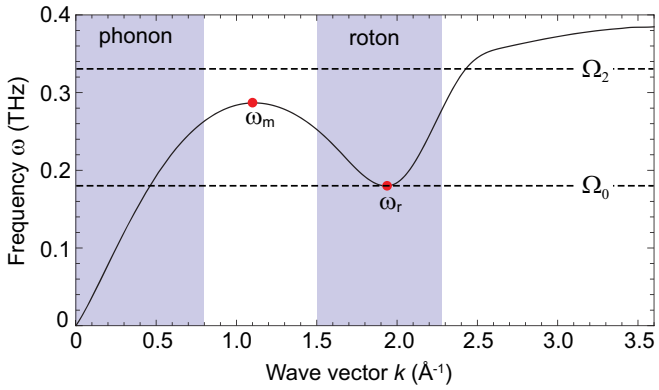


FIG. 1. Dispersion diagram of superfluid He $\omega(k)$ [15]. Two shaded bands correspond to the two types of elementary excitations: phonons and rotons.

interest in Dy spectra in connection with the Bose-Einstein condensation (BEC) [13] and ferrofluidic properties of Dy BEC [14].

## II. THEORETICAL MODEL

According to the bubble model, absorption of a laser photon by the Dy atom will lead to the bubble oscillations damped due to the emission of phonons. In Fig. 1 we plot the dispersion diagram $\omega(k)$ of elementary excitations in superfluid $^4$He [15]. Here, $\omega$ denotes the excitation frequency and $k$ is the wave vector. The density of states (DOS) in the frequency domain is proportional to $(d\omega/dk)^{-1}$:

$$\text{DOS} \propto k(\omega)^2 \left(\frac{d\omega}{dk}\right)^{-1}. \tag{1}$$

The peculiar shape of the dispersion diagram of superfluid He leads to two sharp maxima in the DOS at $\omega_m = 0.29$ THz (maxon) and at $\omega_r = 0.18$ THz (roton), corresponding to $k = 1.1$ and 2.0 Å$^{-1}$, respectively.

We calculate the parameters of the atomic bubble using a standard approach (see, e.g., Refs. [1,16]). The details are given in the Appendix. The Dy-He pair interaction potential is not yet available. We utilize the potential [17] for another lanthanide element Yb that differs from Dy only by the number of electrons in the $4f$ shell. As shown in Ref. [17], the lanthanide-He interaction is dominated by the spherically symmetric outer $6s$ shell and the influence of the anisotropic inner $4f$ shell is rather weak. We therefore neglect the anisotropy and assume the bubble to be spherically symmetric. We found the equilibrium bubble radius $R_b = 5.3$ Å and the eigenfrequencies of undamped bubble oscillations for the breathing and quadrupolar vibration modes, respectively $\Omega_0 = 0.18$ THz and $\Omega_2 = 0.33$ THz. $\Omega_0$ lies very close to the roton frequency $\omega_r$ and is also resonant with the excitations (phonons) from a linear part of the $\omega(k)$ curve having $k \approx 0.5$ Å$^{-1}$. The excitations of both types thus are expected to contribute to the PW spectrum. It was shown in Ref. [4] that bubble vibrations are strongly damped or even overdamped due to the emission of phonons. We therefore do not expect any discrete features associated either with $\Omega_0$ or $\Omega_2$ in the experimental spectra.

We assume that the total atom plus bubble energy for the electronically exited state $U_e(R)$ can be represented by the same curve as that of the ground state $U_g(R)$ shifted to a slightly larger value of the equilibrium radius $R_b^{(e)} = R_b^{(g)} + \delta R$. The value of $\delta R$ determines the intensity ratio of ZPL and PW, but has a little effect on the shape of PW. From the analysis of experimental spectra we infer $\delta R \approx 0.15$ Å (see Appendix).

The knowledge of the parameters of the atomic bubble: $R_b$, $\delta R$, $\alpha$, and the dispersion diagram $\omega(k)$ allows us to model the excitation spectrum using the formalism developed by the authors of Ref. [9] without introducing any further adjustable parameters. Following Ref. [9] we write the wave function $\psi_0^g(r)$ describing the system with the Dy atom and the bubble in the ground state with no phonons excited. $\psi_1^e(k,r)$ corresponds to the excited -state bubble (larger) with a single phonon of the wave vector $k$ excited.

$$\psi_0^{(g)}(r) = \sqrt{\rho(r)}e^{i\varphi} \tag{2}$$

$$\psi_1^{(e)}(k,r) = \sqrt{\rho(r-\delta R)}\frac{\sin(kr+\phi)}{r}e^{i\varphi}. \tag{3}$$

The phase $\phi$ and the set of the allowed values of the wave vector $k$ are determined from the normality and boundary conditions. The wave vector is connected with the phonon frequency via the dispersion relation, as shown in Fig. 1. The probability of a transition between these two states is then given by

$$F_1(k) = \left[4\pi \int \psi_1^{(e)}(k,r)\psi_0^{(g)*}(r)r^2 dr\right]^2. \tag{4}$$

The single-phonon contribution $B_1(\omega)$ to the PW spectrum is produced by a superposition of $F_1(k)$ weighted with the density of states (1). The $n$-phonon contributions $B_n(\omega)$ and the total PW spectrum $G(\omega)$ are obtained [9] from

$$B_n(\omega) = \int B_{n-1}(\omega')B_1(\omega-\omega')d\omega' \tag{5}$$

$$G(\omega) = e^{-S}\sum_n \frac{S^n}{n!}B_n(\omega). \tag{6}$$

Here, $S$ is the Huang-Rhys factor that is related to the intensity of the ZPL via $S = -\ln(I_{\text{ZPL}}/I_{\text{tot}})$.

The main contribution to $G(\omega)$ comes from one-phonon processes. As expected, the PW spectrum is concentrated at 0.17–0.3 THz on the blue side of ZPL and has two sharp peaks corresponding to the two maxima in DOS at $\omega_r$ and $\omega_m$.

Until now, we have assumed that each elementary excitation (phonon) is characterized by a single value of the frequency $\omega$. According to neutron and Raman scattering data [18,19], the phonons and rotons in superfluid He possess a finite spectral width $\gamma$, which increases with temperature. In the temperature range of 1.35–2.1 K, $\gamma$ varies between 4 and 150 GHz [18,19]. The maxon and roton peaks in the PW spectrum are expected to be broadened and smeared out at higher temperatures due to the increase of $\gamma$. We take this effect into account by a convolution of calculated $G(\omega)$ with a Lorenzian with a FWHM equal to 4 and 150 GHz, respectively. The resulting PW spectra are plotted in Fig. 4(b).

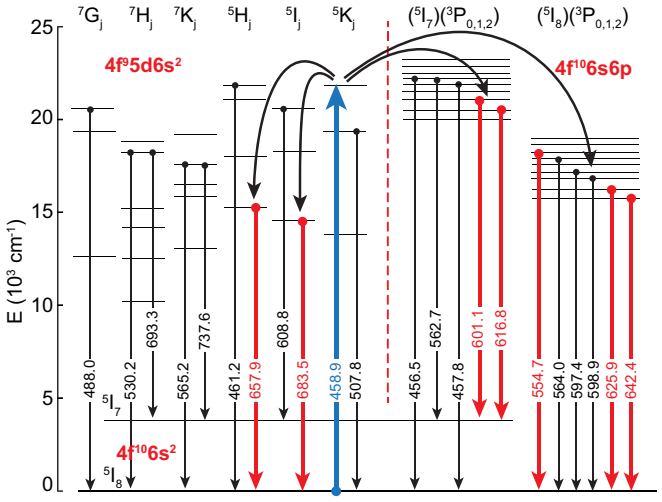


FIG. 2. Electronic states and transitions of Dy atom [21]. Only the groups of states connected by the strong allowed transitions to the two lowest $4f^{10}6s^2$ states are shown. Vertical blue arrow indicates the transition excited by the laser, red arrows indicate the transitions observed in the fluorescence spectrum (see Table I). Transition wavelengths are given in nanometers.

## III. EXPERIMENT

Our experimental setup is similar to that described in our recent paper [20]. A sample cell is filled with liquid He and is immersed in a liquid He bath kept at a temperature of 1.35–2.1 K. Dysprosium atoms are injected into superfluid He by a two-step laser-ablation process using two nanosecond pulsed lasers. First, a metallic Dy target is ablated by a frequency-tripled DPSS laser ($\lambda = 355$ nm) shooting at a repetition rate of 20–50 Hz, with a pulse energy of 70 $\mu$J. This primary ablation produces mostly metal clusters and nanoparticles. Those particles are further dissociated by another frequency-doubled Nd:YAG laser ($\lambda = 532$ nm) with a repetition rate of 10 Hz and a pulse energy of 0.5–15 mJ. This laser is focused in the center of the cell, above the primary ablation target.

Dy atoms in liquid He are excited by a frequency-doubled cw Ti:Sapphire laser aligned along the secondary sputtering laser beam and tuned into the resonance with the transition from the $4f^{10}6s^2\,{}^5I_8$ ground state towards the state $4f^9 5d6s^2\,{}^5K_7$ at $\lambda = 458.9$ nm (see Fig. 2). The transition is thus between the $4f$ and $5d$ shells, screened by the outer $6s$ shell. The fundamental wavelength of the Ti:Sapphire laser is measured by a wavelength meter with an absolute accuracy of $\pm 3.5 \times 10^{-4}$ nm (0.5 GHz). The second harmonic linewidth measured by a Fabry-Perot etalon does not exceed 300 MHz. Laser-induced fluorescence is collected at a right angle with respect to the laser beams and is analyzed with a grating spectrograph (resolution 70 GHz) equipped with a CCD camera and a photomultiplier tube (PMT) for time-resolved measurements.

The ablation process is monitored with a fast digital video camera oriented orthogonal to the laser beams and operated at a frame rate of 500–8500 fps. We observe gas bubbles appearing in the focus of each pulsed laser beam and collapsing within 5–10 ms. We have verified that the emission from the gas bubbles does not contribute to the observed spectroscopic signals.

TABLE I. Spectral shifts, FWHM widths, and relative intensities of electronic transitions of Dy atoms observed in the laser-induced fluorescence spectrum. $\lambda_{free}$ are taken from Ref. [21].

| Transition | $\lambda_{free}$ (nm) | Shift (THz) | FWHM (THz) | $I_{rel}$ |
|---|---|---|---|---|
| $4f^{10}6s^2$-$4f^{10}6s6p$ | 554.7 | 1.05 | 1.02 | 0.017 |
| | 601.1 | 1.17 | 0.90 | 0.007 |
| | 616.8 | 1.17 | 0.84 | 0.002 |
| | 625.9 | 1.05 | 0.84 | 0.113 |
| | 642.4 | 1.14 | 0.93 | 1.00 |
| $4f^{10}6s^2$-$4f^9 5d6s^2$ | 683.5 | −0.54 | 0.15 | 0.052 |
| | 657.9 | −0.54 | 0.15 | 0.002 |

The interaction with the He environment transfers the laser-excited Dy atoms from the $^5K_7$ state to several lower-lying states resulting in a rich emission spectrum. The observed transitions are indicated in Fig. 2 by the red arrows. Their assignments are given in Table I together with the relative intensities $I_{rel}$, spectral shifts with respect to the free-atomic wavelengths $\lambda_{free}$, and the full width at half maximum (FWHM) spectral widths. Five lines belong to the group of $4f^{10}6s^2$-$4f^{10}6s6p$ outer-shell transitions. The line shape of the strongest emission line at $\lambda_{free} = 642.4$ nm is shown in Fig. 3(a). All lines from this group are blue shifted with respect to the free-atomic transitions by ≈1.1 THz and have nearly symmetric Gaussian-like line shapes with a FWHM spectral width of ≈0.9 THz. The line shapes of the two inner-shell $4f^{10}6s^2$-$4f^9 5d6s^2$ transitions are significantly narrower with a FWHM of 150 GHz and have a pronounced asymmetry. Their maxima are red shifted with respect to the corresponding $\lambda_{free}$ by 0.5 THz. The stronger of the two lines at $\lambda_{free} = 683.5$ nm is shown in Fig. 3(b). The line shape can be interpreted as a superposition of a ZPL that is only factor 2 broader than the spectrometer resolution and a red-shifted PW, without any gap between them. This result agrees with the earlier data on Cu and Au [5,10].

The excitation spectrum was obtained by tuning the Ti:Sapphire laser wavelength in steps of 3–10 GHz and recording the full emission spectrum at each point. By plotting the

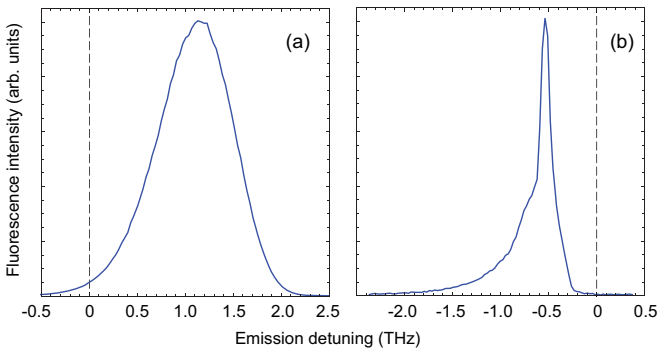


FIG. 3. Emission spectra of Dy atoms in superfluid He. $T = 1.5$ K, excitation at $\lambda_{Las} = 458.9$ nm. (a) valence electron transition $4f^{10}6s^2$-$4f^{10}6s6p$ ($\lambda_{free} = 642.4$ nm); (b) inner-shell transition $4f^{10}6s^2$-$4f^9 5d6s^2$ ($\lambda_{free} = 683.5$ nm). Zero detuning corresponds to $\lambda_{free}$.

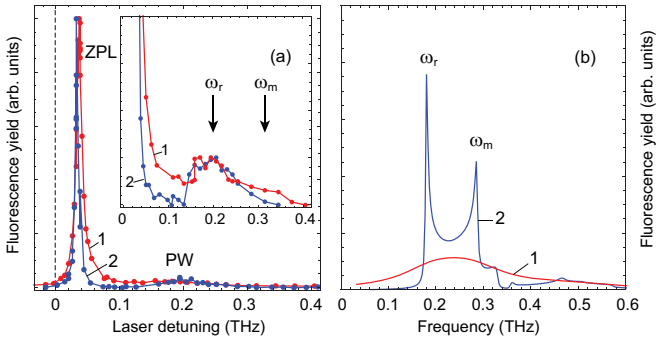


FIG. 4. (a) Low-power excitation spectra of the $4f^{10}6s^2\ {}^5I_8$-$4f^9 5d6s^2\ {}^5K_7$ transition of Dy ($\lambda_{\text{free}} = 458.9$ nm). (b) Calculated PW spectra. In (a) and (b) curve 1: $T = 2.10$ K, curve 2: $T = 1.35$ K.

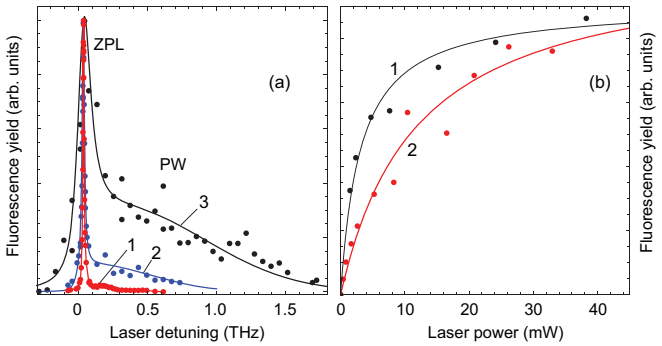


FIG. 5. (a) Normalized excitation spectra of the $4f^{10}6s^2\ {}^5I_8$-$4f^9 5d6s^2\ {}^5K_7$ transition of Dy ($\lambda_{\text{free}} = 458.9$ nm) recorded at different laser intensities. Curve 1: $I_{\text{Las}} = 0.02$ W/cm$^2$, curve 2: $I_{\text{Las}} = 2.5$ W/cm$^2$, curve 3: $I_{\text{Las}} = 17$ W/cm$^2$. (b) Dependence of the fluorescence yield at $\lambda_{\text{Emis}} = 641$ nm on the excitation laser power. Curve 1: excitation of ZPL; curve 2: excitation at the wavelength corresponding to the low-power PW maximum. $T = 2.1$ K; dots: experimental data; lines: fits.

fluorescence yield of different emission lines vs. the excitation wavelength we confirm that all observed emission lines have the same excitation spectrum shown in Fig. 4(a). It consists of a narrow peak with a broad shoulder at the shorter wavelength side, which can be readily attributed to a zero-phonon line and a phonon wing, respectively. The ZPL is blue shifted by ≈30 GHz with respect to the transition in a free Dy atom. At $T = 1.35$ K it has a FWHM spectral width of 4 GHz that is factor 7.5 smaller than that reported in Ref. [3] for Eu. The phonon wing spans approximately 0.3 THz and has a maximum blue shifted with respect to the ZPL by ≈0.17 THz. At low temperature $T = 1.35$ K the intensity of PW rises steeply at a detuning of 110 GHz with respect to ZPL with a pronounced gap between ZPL and PW. The excitation spectrum thus strongly resembles the spectra of glyoxal and other molecules on He nanodroplets [9,22,23] and disagrees with Eu and Tm data in bulk liquid He [2,3]. Increasing helium temperature to $T = 2.1$ K leads to a broadening of ZPL and its shift by ≈3 GHz to higher frequencies. PW is also broadened resulting in an almost complete disappearance of the gap between ZPL and PW.

The dependence of the fluorescence yield on the cw excitation laser power is shown in Fig. 5(b) for two different excitation wavelengths corresponding to the ZPL and to the maximum of PW. There is a pronounced saturation at the laser intensity exceeding ≈0.5 W/cm$^2$. The saturation effect strongly depends on the excitation wavelength: the ZPL saturates at a lower laser power than does the PW. At a high laser power this leads to a significant distortion of the excitation spectrum with a strongly diminished ZPL with respect to the PW. The saturated ZPL also becomes strongly broadened and the gap between ZPL and PW could not be resolved any more. The effect is illustrated in Fig. 5(a). It may explain the puzzling fact that no gap has been observed in earlier studies [2,3] in bulk superfluid He.

The saturation intensity for a homogeneously broadened two-level atomic transition is given [24] by

$$I_S = \frac{1}{\Delta\nu}\frac{\lambda^3}{4\pi ch}\frac{g_k}{g_i}, \tag{7}$$

where $\Delta\nu$ is the transition spectral width, $g_i$, $g_k$ are statistical weights of the two electronic states, $c$ is a speed of light, and $h$ is the Planck constant. Using the measured spectral width of ZPL, we obtain $I_S \approx 10$ W/cm$^2$. In our experiment, the excited-state population is transferred to other excited states. We therefore solve a system of rate equations for the populations in a simplified four-level system including the ground state, the laser-excited ${}^5K_7$ state, and the two lowest states from the $4f^{10}6s6p\ ({}^5I_8)({}^3P_J)$ configuration that produce the most intense fluorescence lines (see Table I). The solution demonstrates that the ground state is depleted and the atoms accumulate the $({}^5I_8)({}^3P_0)$ state ($\lambda_{\text{free}} = 642.4$ nm) whose spontaneous emission rate is the smallest in this group [21,25]. As a result, the fluorescence yield saturates at a lower laser intensity than predicted by Eq. (7).

## IV. DISCUSSION

The maximum of the PW in the experimental absorption spectrum [Fig. 4(a)] is blue shifted from the ZPL by 0.17 THz that is indeed very close to $\omega_r$. No features associated with $\omega_m$ could be distinguished in the experimental PW spectrum. At low temperature, the peak at $\omega_r$ in the calculated spectrum is much narrower than the experimental PW line shape. The same applies to the experimental spectra of glyoxal on He nanodroplets [9]. The discrepancy is not related to the spectral resolution of the experiment. We attribute it to the assumption that the elementary excitations in the vicinity of the atomic bubble are identical to those in bulk superfluid helium. In fact, the PW shape reflects mostly the spectrum of local or pseudolocal excitations existing around the defect. Our atomic bubble calculations show that the characteristic bubble frequencies fall within the phonon-roton spectrum and therefore the bubble vibrations should be considered as pseudolocal modes or wave packets of phonons and rotons. Their spectral width and DOS may differ from those in the bulk.

The gap between ZPL and PW can be observed in various solid matrices, including solid He, but not in classical liquids. A classical hydrodynamic model of atomic bubble vibrations ignoring superfluidity was developed in Ref. [4]. It predicted the spectra without any gap between PW and ZPL. It appears

in superfluid He and in He nanodroplets due to the peculiar structure of the spectrum of the elementary excitations and is thus a manifestation of superfluidity on the nanometer scale.

Although the resolution in our emission spectra is much lower than in excitation, it is clear that the emission spectra of inner-shell transitions [Fig. 3(b)] do not show the same structure as the excitation spectrum. The absence of the gap between the ZPL and PW may indicate the breakdown of superfluidity in the vicinity of the atomic bubble in the process of photon emission.

Due to their sharp ZPL and a large transition dipole, Dy atoms possess a large absorption cross section for the resonant laser light and are therefore good candidates for tracers for the visualization of He flow, similar to $He_2^*$ excimers [26]. We have suppressed the scattered laser light by an interference filter and used the fast video camera to record the atomic fluorescence at 641 nm. We thus obtain a video of the atomic cloud that spreads along the secondary sputtering laser beam after each laser pulse.

In summary, we have measured the temperature dependence of the impurity-phonon coupling in superfluid helium and resolved the longstanding discrepancy between the studies of He nanodroplets [7] and bulk liquid helium [2,3]. The PW in absorption spectrum is peaked at the frequency of the roton peak in the DOS of elementary excitations, which nearly coincides with the breathing vibration mode of the atomic bubble. Increase of the helium temperature leads to the broadening and shift of ZPL and disappearance of the gap between ZPL and PW.

## ACKNOWLEDGMENTS

We thank A. A. Buchachenko for sending us his computed Yb-He interaction potential [17]. This work was supported by Japanese Society for the Promotion of Science KAKENHI Grants No JP24000007 and No. JP17H01145. A.B. acknowledges the financial support from RIKEN internship program.

## APPENDIX

The parameters of the atomic bubble surrounding a Dy atom in superfluid He are calculated using a standard approach (see, e.g., Refs. [1,16]). The bubble is assumed to be spherically symmetric neglecting the small anisotropy of Dy-He interaction [17]. The density of liquid He at the bubble surface is described by a trial function $\rho(r)$ that changes smoothly from zero to the bulk liquid He density $\rho_0$.

$$\begin{aligned}\rho(r) &= 0, \quad r < R_0 \\ &= \rho_0[1-[1+\alpha(r-R_0)]e^{-\alpha(r-R_0)}], \quad r \geqslant R_0. \end{aligned} \tag{A1}$$

The radius of the atomic bubble $R$ is defined as a center of gravity of this interface profile. The parameter $\alpha$ defines the width of the surface layer $b \propto \alpha^{-1}$.

The energy of Dy-He interaction $E_{\rm int}$ is obtained by the integration of the Dy-He pair interactions $U_{\rm pair}(r)$.

$$E_{\rm int}(R_0,\alpha) = 4\pi \int U_{\rm pair}(r)\rho(r)r^2 dr. \tag{A2}$$

The Dy-He interaction potential is not yet available. We therefore utilize the potential [17] for another lanthanide element Yb that is expected to be very similar.

The energy of the bubble $E_{\rm bub}$ is given by

$$E_{\rm bub}(R_0,\alpha) = p\frac{4}{3}\pi R^3 + \kappa 4\pi R^2 + \frac{\pi\hbar^2}{2m}\int \frac{\nabla\rho(r)^2}{\rho(r)} r^2 dr. \tag{A3}$$

Here, $p$ is the hydrostatic He pressure, $\kappa$ is the surface tension parameter, and $m$ is the He atomic mass. The last term represents the energy arising due to the localization of He atoms at the bubble interface.

The total energy $U_g$ is a sum of $E_{\rm int}$ and $E_{\rm bub}$. By minimizing $U_g$ with respect to the parameters $R_0$ and $\alpha$, we find the equilibrium bubble configuration. The equilibrium bubble radius is denoted $R_b$ and is equal to 5.3 Å. The width of the interface profile is $b \approx 1.5$ Å.

We consider breathing and quadrupolar modes of the bubble vibrations. For the breathing mode, the eigenstates $E_{\rm vib}$ and corresponding wave functions $\Psi_g(R)$ are obtained by solving a one-dimensional Schrödinger equation:

$$\left[-\frac{\hbar^2}{2M_0}\frac{d^2}{dR^2} + U_g(R)\right]\Psi(R) = E_{\rm vib}\Psi(R). \tag{A4}$$

The effective mass of the bubble is $M_0 = 4\pi R_b^3\rho_0 m$. It is assumed that the thickness of the bubble interface does not change due to the oscillations. We thus obtain the frequency of the breathing vibrations is $\Omega_0 = 0.18$ THz.

For the quadrupolar mode, we introduce angular dependence of the parameter $R_0$ in Eq. (A1): $R_0(\theta) = R_S + R_Q(3\cos^2\theta - 1)$, where $R_S$ corresponds to the spherical equilibrium configuration. We then reevaluate the total energy as a function of the quadrupolar deformation amplitude $R_Q$ and solve the corresponding Schrödinger equation for the quadrupolar vibrations. In this case, the effective mass of the bubble is $M_2 = R_b^3\rho_0 m/3$. The resulting frequency of the quadrupolar mode is $\Omega_2 = 0.33$ THz.

The interatomic interaction potential corresponding to the electronically excited state is not available. However, it is clear that it is very close to that of the ground state. It is thus reasonable to represent the total atom plus bubble energy for the exited state $U_e(R)$ by the same curve as that of the ground state $U_g(R)$ shifted to a slightly larger value of the equilibrium radius: $U_e(R) = U_g(R-\delta R) + E_0$. Here, $\delta R$ is the difference of equilibrium bubble radii and $E_0$ is the energy of the electronic excitation in a free atom. We write the wave functions of the breathing vibrations in the lower and the upper electronic states, $\Psi_g(v,R)$ and $\Psi_e(v',R)$ and compute the Franck-Condon factors $F(v,v',\delta R)$ for the transitions between the $v = 0$ vibration state of the electronic ground state and all vibration states of the electronically excited state, $v' = 0,1,2,\ldots$.

$$F(v,v',\delta R) = \left[\int \Psi_g(v,R)\Psi_e^*(v',R)dR\right]^2. \tag{A5}$$

In the experimental absorption spectra, the zero-phonon line is formed due to the optical transitions that leave the bubble

vibrations nonexcited. The ZPL intensity $I_{\mathrm{ZPL}}$ is thus proportional to $F(0,0,\delta R)$. All other vibronic transitions contribute to the phonon wing. We therefore write:

$$\frac{I_{\mathrm{ZPL}}}{I_{\mathrm{tot}}} = \frac{F(0,0,\delta R)}{\sum_{v'=0}^{N} F(0,v',\delta R)}. \tag{A6}$$

In fact, due to a small displacement of the two potential curves, only contributions with $v' \leqslant 5$ have to be taken into account. We use $\delta R$ as an adjustable parameter to fit the experimentally observed ratio $I_{\mathrm{ZPL}}/I_{\mathrm{tot}} \approx 0.7$. We thus obtain $\delta R \approx 0.15$ Å.


[1] P. Moroshkin, A. Hofer, and A. Weis, Phys. Rep. **459**, 1 (2008).
[2] K. Ishikawa, A. Hatakeyama, K. Gosyono-o, S. Wada, Y. Takahashi, and T. Yabuzaki, Phys. Rev. B **56**, 780 (1997).
[3] Q. Hui and M. Takami, J. Low Temp. Phys. **119**, 393 (2000).
[4] P. Moroshkin, V. Lebedev, and A. Weis, Europhys. Lett. **96**, 26002 (2011).
[5] P. Moroshkin, V. Lebedev, and A. Weis, J. Chem. Phys. **139**, 104307 (2013).
[6] D. Hsu and J. L. Skinner, J. Chem. Phys. **81**, 1604 (1984).
[7] J. P. Toennies and A. F. Vilesov, Angew. Chem. Int. Ed. **43**, 2622 (2004).
[8] C. Callegari and W. E. Ernst, in *Handbook of High-Resolution Spectroscopy*, edited by M. Quack and F. Merkt (Wiley, New York, 2011), Vol. 3, pp. 1551–1594.
[9] M. Hartmann, F. Mielke, J. P. Toennies, A. F. Vilesov, and G. Benedek, Phys. Rev. Lett. **76**, 4560 (1996).
[10] P. Moroshkin, V. Lebedev, and A. Weis, Phys. Rev. A **84**, 052519 (2011).
[11] P. Moroshkin, V. Lebedev, and A. Weis, J. Low Temp. Phys. **162**, 710 (2011).
[12] M. Lemeshko, N. Y. Yao, A. V. Gorshkov, H. Weimer, S. D. Bennett, T. Momose, and S. Gopalakrishnan, Phys. Rev. B **88**, 014426 (2013).
[13] M. Lu, N. Q. Burdick, S. H. Youn, and B. L. Lev, Phys. Rev. Lett. **107**, 190401 (2011).
[14] H. Kadau, M. Schmitt, M. Wenzel, C. Wink, T. Maier, I. Ferrier-Barbut, and T. Pfau, Nature (London) **530**, 194 (2016).
[15] R. J. Donnelly and C. F. Barenghi, J. Phys. Chem. Ref. Data **27**, 1217 (1998).
[16] T. Kinoshita, K. Fukuda, Y. Takahashi, and T. Yabuzaki, Phys. Rev. A **52**, 2707 (1995).
[17] A. A. Buchachenko, G. Chalasinski, and M. M. Szczesniak, Eur. Phys. J. D **45**, 147 (2007).
[18] A. D. B. Woods and R. A. Cowley, Rep. Prog. Phys. **36**, 1135 (1973).
[19] M. R. Gibbs, K. H. Andersen, W. G. Stirling, and H. Schober, J. Phys. Cond. Matt. **11**, 603 (1999).
[20] P. Moroshkin and K. Kono, Phys. Rev. A **93**, 052510 (2016).
[21] A. Kramida, Yu. Ralchenko, J. Reader, and NIST ASD Team, NIST Atomic Spectra Database (ver. 5.3), [Online]. http://physics.nist.gov/asd [2017, February 27]. National Institute of Standards and Technology, Gaithersburg, 2015.
[22] M. Hartmann, A. Lindinger, J. P. Toennies, and A. F. Vilesov, Phys. Chem. Chem. Phys. **4**, 4839 (2002).
[23] R. Lehnig and A. Slenczka, J. Chem. Phys. **122**, 244317 (2005).
[24] W. Demtröder, *Laser Spectroscopy* (Springer, Berlin, 2008).
[25] V. A. Komarovskii, Opt. Spectrosc. **71**, 322 (1991) [Opt. Spektrosk. **71**, 559 (1991)].
[26] W. Guo, S. B. Cahn, J. A. Nikkel, W. F. Vinen, and D. N. McKinsey, Phys. Rev. Lett. **105**, 045301 (2010).